Proceedings of the Fifteenth International Conference on
Computational Structures Technology
Edited by: P. Iványi, J. Kruis and B.H.V. Topping
Civil-Comp Conferences, Volume 9, Paper 13.2
Civil-Comp Press, Edinburgh, United Kingdom, 2024
ISSN: 2753-3239, doi: 10.4203/ccc.9.13.2

Stress and Free Vibration Analysis of Fibre-Reinforced Soft Structures by 2D High Order Finite Elements

A. Pagani, P. Chiaia and E. Carrera

**Department of Mechanical and Aerospace Engineering,
Politecnico di Torino, Italy**

Abstract

This study explores higher-order 2D plate finite elements for the stress and modal analysis of soft structures. The problem is established within the domain of the Carrera Unified Formulation (CUF), integrating available hyperelastic models in a unified, fully nonlinear Finite Element (FE) approach under a Total Lagrangian formulation. The matrix form of the governing equations for the nonlinear static and free vibration analysis is carried out through the Principle of Virtual Displacements (PVD), obtaining a pure displacement-based FE model. The numerical procedure is based on a Newton-Raphson linearization approach and path-following methods. The primary objective of this research is to analyze the three-dimensional stress state of soft structures in the large strain regime and how highly nonlinear pre-stressed conditions affect natural frequencies and modal shapes. The proposed results are compared with the FE solution obtained through classical models available in commercial software. The numerical results proposed assess the efficiency of the accuracy of higher-order 2D models for displacements, strains, and modal behaviour of soft structures.

Keywords: hyperelastic materials, soft materials, high-order plate theories, finite elements method, free vibration, stress analysis.

1 Introduction

Hyperelastic materials are a class characterized by their ability to undergo large elastic deformations and return to their original configuration upon removing loads. Soft material behaviour is typically characterized by a nonlinear stress-strain relationship. Due to their unique properties, hyperelastic materials play a crucial role in engineering and biomechanics. In the aerospace industry, hyperelastic materials are used to design flexible seals, vibration dampers, and impact-resistant components. The capabilities of such materials are explored when extreme environmental conditions and dynamic loads are considered [2].

In mechanical and civil engineering, hyperelastic materials are explored in products such as automotive tyres, seals, gaskets, and various elastomeric components [4]. Their unique capability to absorb and dissipate energy significantly enhances the performance and durability of mechanical systems, providing resistance to wear and fatigue. For these reasons, typically, seismic isolation bearings and bridge bearings are designed adopting hyperelastic soft materials, where their flexibility and resilience are essential in energy dissipation [5].

Hyperelastic materials are extensively used in the field of biomechanics to model biological tissues [6], such as skin, tendons, and ligaments, which can undergo large strains while maintaining their integrity. This unique characteristic is of utmost importance in the design of medical devices, prosthetics, and implants, where biocompatibility and durability under physiological conditions are essential [7].

Given the complex behaviour of hyperelastic materials, accurate mathematical modelling is crucial for effective design and applications [9]. Accurate models for large strain analysis are essential in widely adopting finite element (FE) models, which provide a powerful computational approach for simulating complex structures with various loads and boundary conditions. The geometric and material nonlinearities considered in the hyperelastic material modelling require high-fidelity FE models, especially when incompressible materials are considered [8]. The classical limitations of FE models are enhanced in hyperelasticity, where volumetric locking arises due to incompressibility. It is generally possible to deal with these limitations by adopting higher-order structural theories, avoiding classical FE formulations, or hybrid FE formulations [10].

For this reason, this work presents a high-order 2D plate model based on refined structural theory. Within the well-established Carrera Unified Formulation framework, high-order 2D plate models for the static and modal analysis of multilayered fibre-reinforced soft materials are defined [23]. Under the CUF formalism, the three-dimensional displacement field is provided in a formal expression independent of the structural theory adopted [14], allowing the definition of the matrix-form governing equations in terms of Fundamental Nuclei (FN), which are invariants of the kinematic model and theory of structure approximation adopted. The full Green-Lagrange strain tensor is considered to model large strain problems [21]. The nonlinear governing equations are solved through a Newton-Raphson linearized procedure and path-

following methods. In this unified framework, the nonlinear static and modal analyses around non-trivial equilibrium states are defined, adopting the same formalism. The effects of the mathematical model adopted, both for the static and modal analysis, are analyzed for different discretization and theory of structure approximation since the latter is now an input parameter of the FE model.

The work is organized as follows: (i) first, the hyperelastic constitutive law are is presented in Sec. 2, presenting the nonlinear stress-strain relations for isotropic and isotropic soft materials ; (ii) second, unified 2D plate models are described in Sec. 3; (iii) subsequently, the nonlinear governing equations for the static and modal static analysis in nontrivial equilibrium states are presented in Sec. 4, where the Principle of Virtual Displacements is exploited to derive the Fundamental Nuclei (FN) of FE matrices; (iv) actual numerical results and analysis of different benchmark problems through refined 1D models are discussed in Sec. 5, presenting the accuracy of our models in the analysis of compressible and nearly-incompressible structures; (v) finally, the conclusions are discussed in Sec. 6.

2 Hyperelastic constitutive modeling

Soft material behavior is modeled in the hyperelastic framework based on strain energy function approach. Given the deformation gradient $\mathbf{F}$ and consequently the right Cauchy-Green strain tensor $\mathbf{C}$, the hyperelastic constitutive law is written as:

$$\mathbf{S} = 2\frac{\partial \Psi(\mathbf{C})}{\partial \mathbf{C}} \tag{1}$$

where $\mathbf{S}$ is the secon Piola-Kirchoff stress tensor and Ψ is the strain energy density function per unit volume. In the present work, both isotropic and fibre-reinforced soft materials are considered. In general, these constitutive models are assigned, defining the strain energy function Ψ in terms of the invariants (I_1, I_2, I_3) of right Cauchy-Green tensor $\mathbf{C}$, and specific pseudo-invariants of the deformation depending on the fibre-reinforcement effect [12]:

$$\Psi = \Psi(I_1(\mathbf{C}), I_2(\mathbf{C}), I_3(\mathbf{C}), I_4(\mathbf{C}, \mathbf{a}_0), I_5(\mathbf{C}, \mathbf{a}_0)) \tag{2}$$

In a nonlinear finite element scenario, where both large strain and nonlinear constitutive laws are taken into account, the incremental approach is adopted. In the hyperelastic constitutive modeling, the constitutive law Eq. (1) can be linearizedm defining the tangent elasticity tensor:

$$\Delta \mathbf{S} = \mathbb{C} : \frac{1}{2}\Delta \mathbf{C} = \mathbb{C} : \Delta \mathbf{E} \tag{3}$$

where $\mathbb{C}$ is the tangent elasticity tensor. More details about the derivation of the analytic expression of the tangent elasticity tensor $\mathbb{C}$ under the coupled and decoupled approach can be found in [12, 13].

$$\mathbb{C} = 2\frac{\partial \mathbf{S}(\mathbf{C})}{\partial \mathbf{C}} = \frac{\partial \mathbf{S}(\mathbf{E})}{\partial \mathbf{E}} = 4\frac{\partial^2 \Psi}{\partial \mathbf{C} \partial \mathbf{C}} \tag{4}$$

3 High order plate models

The present high-order plate models are defined in the well-established CUF framework. The reader is addressed to Carrera *et al.* [14] for an extensive description of the present unified finite element models. In the unified formulation of plate theories, the displacement field is provided as a formal expression independent of the plate structural theory considered

$$\mathbf{u}(x, y, z) = F_\tau(z)\mathbf{u}_\tau(x, y) \qquad \tau = 1, ..., M \tag{5}$$

where F_τ is the set of structural theory expansion polynomials, defined along the plate thickness, M is related to the order of the theory of structure adopted, which is an input parameter of the analysis and $\mathbf{u}_\tau$ is the vector of generalized displacement components along the plate mid-surface. Adopting this formal expression of the displacement field, any structural theory can be exploited in defining the displacement field without any loss of generality. In the following, the Einstein notation is adopted; thus, the index τ is used to indicate summation. The capabilities of high-order 2D CUF plate models for multilayered structures are established in the literature; the reader is addressed to [15–18] for more details. 2D CUF models based on Lagrange Expansion (LE models) are investigated here. In general, this approach defines a local independent displacement field for each plate sub-layer. For this reason, LE models are also addressed as a Layer-Wise (LW) approach in resulting FE models where the generalized unknowns describe exactly the three-dimensional components of the displacement field [14]. After that, once the structural theory adopted is assigned, the generalized unknowns along the plate mid-surface $\mathbf{u}_\tau(x, y)$ are further discretized by adopting the classical FE approach:

$$\mathbf{u}_\tau(y) = N_i(x, y)\mathbf{u}_{\tau i} \qquad i = 1, ..., N_n \tag{6}$$

where $\mathbf{u}_{\tau i}$ are the final unknowns of the problem corresponding to the nodal displacement components, $N_i(x, y)$ the classical 2D shape functions and N_n is the total number of finite nodes of the element adopted. The final expression of the 3-D displacement field in the CUF domain can be seen as a coupled expansion of structural plate theories and kinematic models along the plate mid-surface, modelled in a single unified expression of the displacement field:

$$\mathbf{u}(x, y, z) = F_\tau(z)\mathbf{u}_\tau(x, y) = F_\tau(z)N_i(x, y)\mathbf{u}_{\tau i} \tag{7}$$

The classical 2D shape functions will be addressed as linear Q4, parabolic Q9, and cubic Q16 finite interpolation along the plate mid-surface, explicitly indicating the total number of finite nodes adopted. Equation (7) is the most general expression of the 3D displacement field, independent from the general higher-order structural theory adopted and kinematic models. In this way, a hierarchical implementation of any finite element model is described, obtaining the specific model by assigning the two independent polynomial bases for the plate mid-surface kinematics and theory of structure approximation. In LW models, displacement continuity is achieved from

an FE matrix assembling point of view [19], imposing displacement continuity at the nodal level. The implementation of high-order plate models can efficiently predict accurate 3D stress distributions, avoiding inconsistent solutions when transverse out-of-plane stresses are considered [20].

4 Nonlinear governing equations

The nonlinear equilibrium equations in matrix form are carried out through the Principle of Virtual Displacements (PVD), which states:

$$\delta\mathcal{L}_{ine} + \delta\mathcal{L}_{int} = \delta\mathcal{L}_{ext} \tag{8}$$

where $\delta\mathcal{L}_{ine}$ is the inertial load, $\delta\mathcal{L}_{int}$ and $\delta\mathcal{L}_{ext}$ are the internal strain energy and external loads, respectively. In a CUF-based finite element scenario, implementing the index notation for real and virtual measures for the full Green-Lagrange strain tensor, the governing equations are provided in terms of Fundamental Nuclei (FN) of the internal and external force vectors and mass matrix:

$$\delta\mathbf{u}_{sj}: \quad \mathbf{M}^{\tau sij}\ddot{\mathbf{u}}_{\tau i} + \mathbf{F}_{int}^{sj} = \mathbf{F}_{ext}^{sj} \quad \rightarrow \quad \mathbf{M}\ddot{\mathbf{u}} + \mathbf{F}_{int} = \mathbf{F}_{ext} \tag{9}$$

$$\varphi_{res}(\mathbf{u}, \ddot{\mathbf{u}}, \mathbf{f}) = \mathbf{M}\ddot{\mathbf{u}} + \mathbf{F}_{int} - \mathbf{F}_{ext} \tag{10}$$

The nonlinear problem is solved through the minimization of the unbalanced nodal forces vector, $\varphi_{res}(\mathbf{u}, \ddot{\mathbf{u}}, \mathbf{f})$, that is then linearized to implement incremental numerical solver based on path-following constraint [22]. In this context, the incremental equation obtained considering a Taylor expansion truncated at the first order is then rearranged, defining the tangent stiffness matrix, and under the hypothesis of constant mass matrix and conservative loads [23]:

$$\mathbf{M}\Delta\ddot{\mathbf{u}} + \mathbf{K}_T\Delta\mathbf{u} = -\varphi_{res}(\mathbf{u}_0, \ddot{\mathbf{u}}_0, \mathbf{f}_0) + \mathbf{I}\Delta\lambda\mathbf{f}_{ref} \tag{11}$$

Starting from Eq. (11), one can define the classical nonlinear static problem, in which the two incremental unknowns are coupled with an additional constraint equation:

$$\begin{cases} \mathbf{K}_T\Delta\mathbf{u} = -\varphi_{res}(\mathbf{u}_0, \ddot{\mathbf{u}}_0, \mathbf{f}_0) + \Delta\lambda\mathbf{f}_{ref} \\ c(\Delta\mathbf{u}, \Delta\mathbf{f}) = 0 \end{cases} \tag{12}$$

Subsequently, in the computed non-trivial equilibrium state, imposing a harmonic increment of the type $\Delta\mathbf{u} = \mathbf{\Phi}e^{i\omega t}$, the linear eigenvalue problem that gives the natural frequencies and the normal modes of vibration in the pre-stressed state is:

$$(\mathbf{K}_T - \omega^2\mathbf{M})\mathbf{\Phi} = 0 \tag{13}$$

The reader is addressed to Pagani *et al.* [23] for the complete derivation of the undamped vibration problem around non-trivial equilibrium states for hyperelastic soft structures.

5 Numerical results

The first case study analyzes a multilayered clamped square plate of compressible silicon rubber modelled in the hyperelastic framework. In the following, both a nonlinear static analysis and subsequent modal analysis around non-trivial equilibrium states are performed; a square plate with a lateral side of $L = 1$ m and thickness ratio $L/h = 10$ is made of two equal-thickness layers. Here, two different LE models, the LE2 parabolic and LE3 cubic expansion models, are adopted in the thickness direction. The present case study's geometrical features and boundary conditions are depicted in Fig. 1.

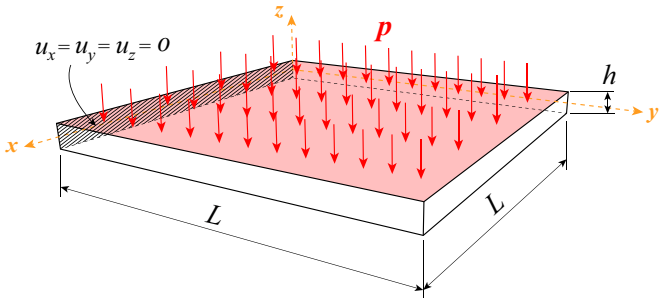

Figure 1: Cantilever multilayered silicon plate: geometrical features and boundary conditions.

Each hyperelastic layer is described adopting the decoupled Mooney-Rivlin model for the isochoric component and the classical quadratic model for the volumetric component of the strain energy function:

$$\Psi = \Psi_{vol}(J) + \bar{\Psi}(\bar{I}_1, \bar{I}_2) = \frac{1}{D_1}(J-1)^2 + c_{10}(\bar{I}_1 - 3) + c_{01}(\bar{I}_2 - 3) \quad (14)$$

From bottom to top, the global stacking sequence is considered A/B, and the material parameters adopted are listed in Table 1. In the subsequent investigations, the material density of the hyperelastic beam is set to a typical value for silicone rubber ($\rho = 2330$ kg/m^3).

The first numerical investigation is the convergence analysis for the nonlinear static

	c_{10} [MPa]	c_{01} [MPa]	μ [MPa]	ν [-]	E [MPa]	$D_1 = 2/k$ [MPa^{-1}]
Material A	30	-4	52	0.2	124.8	$2.8846 \cdot 10^{-2}$
Material B	10	1.5	23	0.3	59.8	$4.0133 \cdot 10^{-2}$

Table 1: Cantilever multilayered silicon plate: material properties.

analysis. The accuracy and the efficiency of the proposed models are assessed, measuring the accuracy in terms of the relative error to the reference solution and the computational costs in terms of total degrees of freedom (DOF) required by the simulation. The thin plate is investigated under a uniform transversal pressure, analyzing

the non-trivial equilibrium states of the structure. Table 2 shows the comparison between 2D CUF model results and full 3D ABAQUS models, analyzing the transversal displacement u_z measured at the point $(L, L/2, h)$ at the top surface. The effect of the finite element discretization along the plate mid-surface and the theory of structure approximation are discussed here. All the mathematical models employ N parabolic (LE2) or cubic (LE3) expansion models for each layer. From the analysis proposed, the equilibrium path is correctly predicted by each model in the small displacement regime, also for coarse discretization. Instead, refined discretizations along the plate mid-surface are required to predict accurately highly nonlinear equilibrium states. In terms of displacement analysis, the effects of the theory of structure approximation are not evident due to the geometrical features of the plate. In all the cases, the most accurate model involves 20x20 parabolic Q9 elements along the plate mid-surface. Figure 2(a) shows the global equilibrium path when only parabolic models are considered in the thickness expansion, instead Fig. 2(b) shows the same equilibrium paths when cubic model along the thickness are considered, comparing in both cases the results with the full 3D ABAQUS solution. Results perfectly match refined discretization. However, minor differences are observed for coarse discretization along the plate mid-surface.

Furthermore, in the trivial equilibrium condition, the natural frequencies are analyzed, solving the classical linear eigenvalue problem. Table 3 shows the first five natural frequencies, employing the most accurate discretization evinced in the previous convergence analysis. Results are in excellent agreement with the proposed reference, with an evident save in total DOF employed by the simulation.

Finally, the behaviour of natural frequencies along the equilibrium path and the effect of the pre-stressed condition in the non-trivial equilibrium state is analyzed by solving Eq. (13) for each computed equilibrium condition. Figure 3 shows the first ten natural frequencies and their behaviour for increasing the value of applied transversal pressure. Slight modal interactions are observed at the moderate displacement regime between higher-order modes.

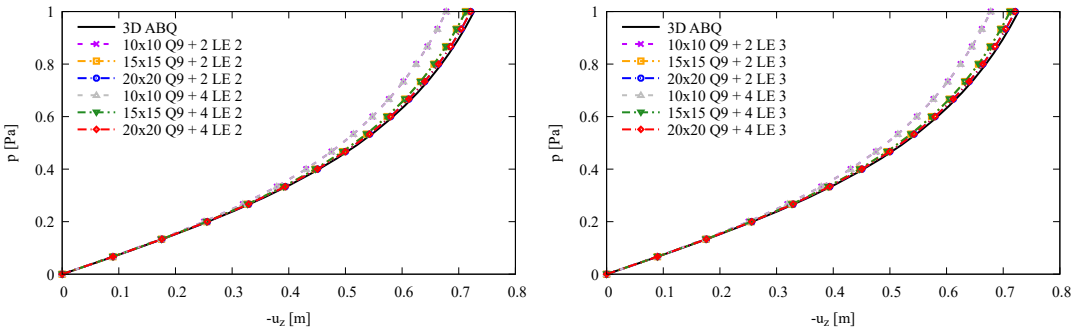

(a) Parabolic model

(b) Cubic model

Figure 2: Cantilever compressible silicon plate: equilibrium paths.

		$-\mathbf{u_z}$(L/2,L,h) [mm]				
Q9	**Expansion**	**p = 16 Pa**	**p = 32 Pa**	**p = 48 Pa**	**p = 64 Pa**	**DOF**
10x10	2 LE 2	$0.25051^{(2.58\%)}$	$0.43064^{(4.97\%)}$	$0.54759^{(6.21\%)}$	$0.62480^{(6.66\%)}$	6615
	2 LE 3	$0.25051^{(2.58\%)}$	$0.43064^{(4.97\%)}$	$0.54759^{(6.21\%)}$	$0.62480^{(6.66\%)}$	9261
	4 LE 2	$0.25051^{(2.58\%)}$	$0.43064^{(4.97\%)}$	$0.54759^{(6.21\%)}$	$0.62480^{(6.66\%)}$	11097
	4 LE 3	$0.25051^{(2.58\%)}$	$0.43064^{(4.97\%)}$	$0.54759^{(6.21\%)}$	$0.62480^{(6.66\%)}$	17199
15x15	2 LE 2	$0.25515^{(0.78\%)}$	$0.44683^{(1.39\%)}$	$0.57357^{(1.76\%)}$	$0.65643^{(1.93\%)}$	14415
	2 LE 3	$0.25515^{(0.78\%)}$	$0.44683^{(1.39\%)}$	$0.57357^{(1.76\%)}$	$0.65643^{(1.93\%)}$	20181
	4 LE 2	$0.25515^{(0.78\%)}$	$0.44683^{(1.39\%)}$	$0.57357^{(1.76\%)}$	$0.65643^{(1.93\%)}$	25947
	4 LE 3	$0.25515^{(0.78\%)}$	$0.44683^{(1.39\%)}$	$0.57357^{(1.76\%)}$	$0.65643^{(1.93\%)}$	37479
20x20	2 LE 2	$0.25629^{(0.34\%)}$	$0.45058^{(0.57\%)}$	$0.57978^{(0.69\%)}$	$0.66427^{(0.76\%)}$	25215
	2 LE 3	$0.25629^{(0.33\%)}$	$0.45058^{(0.57\%)}$	$0.57978^{(0.69\%)}$	$0.66427^{(0.76\%)}$	35301
	4 LE 2	$0.25629^{(0.33\%)}$	$0.45058^{(0.57\%)}$	$0.57978^{(0.69\%)}$	$0.66427^{(0.76\%)}$	45387
	4 LE 3	$0.25629^{(0.33\%)}$	$0.45058^{(0.57\%)}$	$0.57978^{(0.69\%)}$	$0.66427^{(0.76\%)}$	66559
3D ABQ	20000 C8D20R	0.25715	0.45315	0.58382	0.66935	334815

Table 2: Cantilever multilayered silicon plate: convergence analysis. Transversal displacement $-u_z$ [mm].

Expansion	**Mode 1**	**Mode 2**	**Mode 3**	**Mode 4**	**Mode 5**	**DOF**
2 LE 2	$0.31489^{(0.18\%)}$	$0.78380^{(0.28\%)}$	$1.94471^{(0.35\%)}$	$2.46886^{(0.21\%)}$	$2.83801^{(0.40\%)}$	25215
2 LE 3	$0.31489^{(0.18\%)}$	$0.78379^{(0.28\%)}$	$1.94468^{(0.35\%)}$	$2.46882^{(0.21\%)}$	$2.83793^{(0.40\%)}$	35301
4 LE 2	$0.31489^{(0.18\%)}$	$0.78379^{(0.28\%)}$	$1.94468^{(0.35\%)}$	$2.46882^{(0.21\%)}$	$2.83794^{(0.40\%)}$	45387
4 LE 3	$0.31489^{(0.18\%)}$	$0.78379^{(0.28\%)}$	$1.94468^{(0.35\%)}$	$2.46882^{(0.21\%)}$	$2.83794^{(0.40\%)}$	65559
20000 C8D20R	0.31432	0.78163	1.93798	2.46366	2.82670	334815

Table 3: Cantilever multilayered silicon plate: convergence analysis on the first fifth normal modes of vibration around the trivial conditions [Hz].

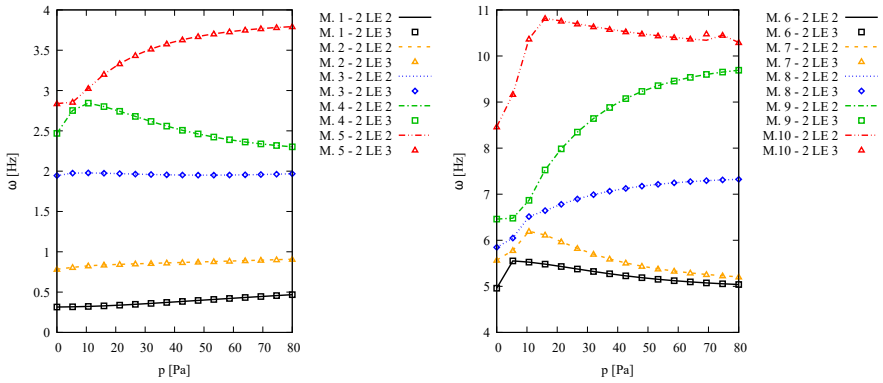

(a) Modes 1-5 (b) Modes 6-10

Figure 3: Compressible silicon plate; natural frequencies for increasing pressure.

5.1 Circular plate under uniform transversal pressure

The static and modal analysis of a clamped circular plate made of fibre-reinforced hyperelastic materials is analyzed as a second numerical example. The plate, of radius $R = 50$ mm and thickness $h = 5$ mm, is clamped at its lateral surface and subjected to a vertical transversal pressure $\mathbf{q}_z$. Figure 4(a) depicts the geometrical features and boundary conditions.

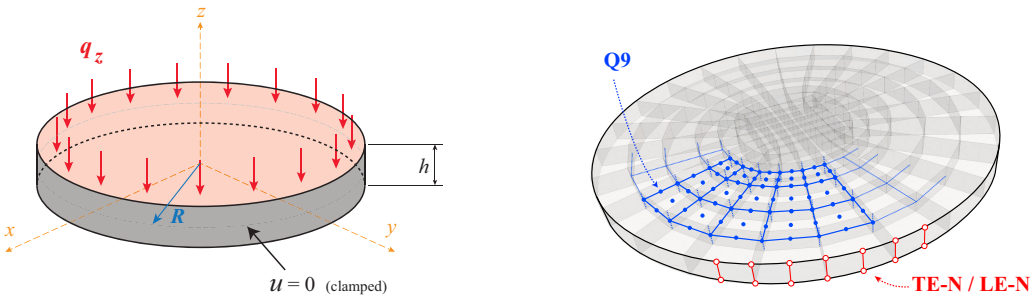

(a) Geometry and boundary conditions.

(b) Mathematical model description.

Figure 4: Compressible circular plate: configuration of the case study and discretization adopted.

The material model is a compressible Neo-Hookean model coupled with the quadratic volumetric and fibre-reinforcement strain energy functions:

$$\Psi(\mathbf{C}) = \frac{\mu}{2}(I_1 - 3) + \frac{\lambda}{2}(J-1)^2 - \mu \log J + \gamma(I_4 - 1)^2 \tag{15}$$

The material constants are fixed to $\mu = 1$ MPa, $\lambda = 4$ MPa and $\gamma = 0.375$ MPa, as reported in the reference case study.

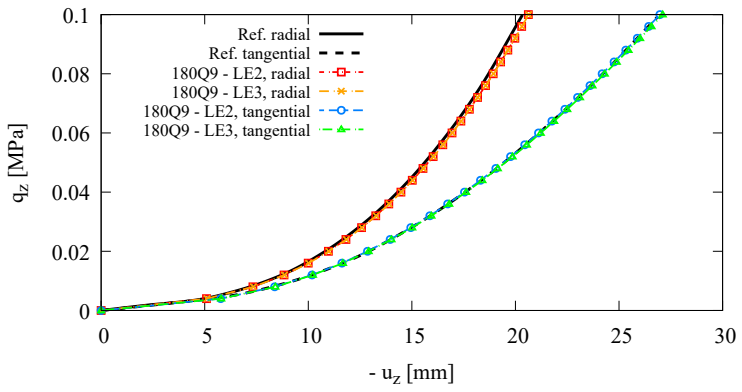

Figure 5: Compressible circular plate: equilibrium path.

The analysis proposed aims to investigate the effects of fibre distributions on the static and modal behaviour and the influence of the discretization along the thickness when

two different fibre distributions are considered: radial and tangential fibre orientation. This case study has been recently proposed by Beheshti *et al.* [24] and analyzed by Chiaia *et. al* [13].

The nonlinear static analysis of the structure is proposed in both fibre distributions considered. In particular, the vertical displacement $-u_z$ measured at the plate centre is analyzed. The results, in terms of equilibrium paths, proposed in Fig. 5 have been carried out adopting previously investigated convergent mesh made by 180 Q9 parabolic elements along the plate mid-surface and analyzing the effect of the theory of structure approximation on the results, when 1 LE2 parabolic and 1 LE3 cubic model along the thickness are considered. In this case, the results perfectly match the reference benchmark in both fibre configurations. Minor differences are observed at highly nonlinear conditions in the case of radial fibre distribution. In particular, a stiffer behaviour is observed in the case of radial fibre distribution.

Thereafter, the natural frequencies are investigated in the marked computed non-trivial equilibrium states, solving the linear eigenvalue problem Eq. (13) again for each equilibrium condition. Figure 6 shows the variation of the first ten natural frequencies along the equilibrium path when the radial fibre distribution case is considered, analyzing the predicted behaviour and comparing the results obtained adopting the two thickness discretization employed before. The same comparison is proposed in the case of tangential fibre distribution and shown in Fig. 7.

In general, results suggest that natural frequencies increase along the equilibrium path due to the stiffening behaviour observed in the equilibrium path Fig. 5. The radial fibre-distribution configuration leads to a stiffer global behaviour of the plate in terms of static and modal response. Natural frequencies are higher than the tangential distribution cases. More evident modal interactions are instead observed in the tangential distribution case. Also, the increase in natural frequency is smaller than the radial distribution case.

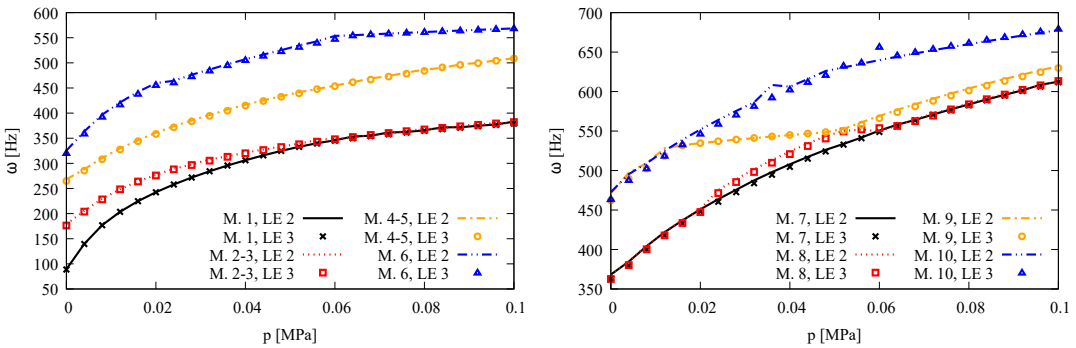

(a) Modes 1-6

(b) Modes 7-10

Figure 6: Compressible circular plate: radial fibre configuration, variation of the first ten natural frequencies along the equilibrium path.

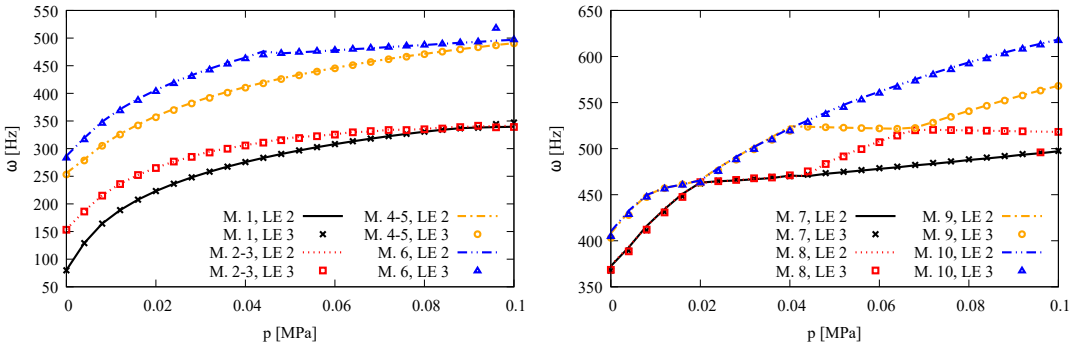

(a) Modes 1-6

(b) Modes 7-10

Figure 7: Compressible circular plate: tangential fibre configuration, variation of the first ten natural frequencies along the equilibrium path.

6 Concluding remarks

This paper introduces the unified plate finite element models based on Carrera Unified Formulation (CUF) for the static and modal analysis of multilayered anisotropic hyperelastic plate structures. The mechanical behaviour of isotropic and fibre-reinforced soft materials has been described in the classical continuum mechanics framework for hyperelasticity, introducing the isotropic and direction-dependent invariants of the deformations from which the definition of strain energy density function depends.

The finite element (FE) model introduced in the present work is based on CUF, a framework in which the displacement field is provided as a formal expression independent of the theories of structure approximation adopted.

The matrix-form nonlinear governing equations have been derived by the Principle of Virtual Displacement (PVD), imposing the CUF formalism, providing the FE matrices involved in the nonlinear problem in terms of Fundamental Nuclei (FN), invariants of the kinematics assumptions of the FE model adopted. Starting from the same derivation procedure, both the static nonlinear problem and the eigenvalue problem of the modal analysis around non-trivial equilibrium states are defined. The static nonlinear problem is solved using the Newton-Raphson iterative procedure coupled with load-control procedures or arc-length constraints.

The proposed unified plate finite element models have been tested and compared with benchmark solutions in the literature or results from classical FE formulations. The results demonstrate the accuracy and efficiency of the present implementation of higher-order plate theories in a unified FE model, offering a significant reduction in computational costs required by the simulation, which is a crucial factor in practical applications.

Future research will extend the present approach to the analysis of orthotropic hyperelastic media adopting higher-order 1D beam and 2D plate/shell models, analyzing the displacement and stress fields of soft fibrous structures with two families of fibres.

Furthermore, detailed analyses of locking phenomena, and numerical investigations about volumetric locking, are intended, exploring refined mathematical models introduced to deal with these problems such as the hybrid formulation (or u/p formulation) in the unified approach of 1D and 2D CUF-based models.

Acknowledgements

This project has received funding from the European Research Council (ERC) under the European Union's Horizon 2020 research and innovation programme (Grant agreement No. 850437).

References

[1] R.W. Ogden, Large deformation isotropic elasticity – on the correlation of theory and experiment for incompressible rubberlike solids, Proc. R. Soc. Lond. Ser. A Math. Phys. Eng. Sci. 326 (1567) (1972) 565–584, http://dx.doi.org/10.1098/rspa.1972.0026.

[2] Mansouri M.R., Beter J., Fuchs P.F., Schrittesser B., and Pinter G. Quantifying matrix-fiber mechanical interactions in hyperelastic materials. International Journal of Mechanical Sciences, 195:106268, April 2021, DOI: 10.1016/j.ijmecsci.2021.106268.

[3] Guo L., Lv Y., Deng Z., Wang Y., and Zan X. Tension testing of silicone rubber at high strain rates. Polymer Testing, 50:270–275, April 2016, DOI: 10.1016/j.polymertesting.2016.01.021.

[4] Chebbi E., Wali M., and Dammak F. An anisotropic hyperelastic constitutive model for short glass fiber-reinforced polyamide. International Journal of Engineering Science, 106:262–272, September 2016, DOI: 10.1016/j.ijengsci.2016.07.003.

[5] Amabili M. Nonlinear damping in large-amplitude vibrations: modelling and experiments. Nonlinear Dynamics, 93(1):5–18, October 2017, DOI: 10.1007/s11071-017-3889-z.

[6] Nitti A., Kiendl J., Gizzi A., Reali A., and De Tullio M.D. A curvilinear isogeometric framework for the electromechanical activation of thin muscular tissues. Computer Methods in Applied Mechanics and Engineering, 382:113877, August 2021, DOI: 10.1016/j.cma.2021.113877.

[7] Canales C., Garcia-Herrera C., Rivera E., Macias D., and Celentano D. Anisotropic hyperelastic material characterization: Stability criterion and inverse calibration with evolutionary strategies. Mathematics, 11(4):922, feb 2023.

[8] Van Huyssteen D and Reddy B.D. A virtual element method for transversely isotropic hyperelasticity. Computer Methods in Applied Mechanics and Engineering, 386:114108, December 2021, DOI: 10.1016/j.cma.2021.114108.

[9] Velayati H.R. and Kordkheili S.A.H. A particular manner to observe free-edge effects in hybrid elastomer/composites plates. Composites Part C: Open Access, 11:100369, July 2023, DOI: 10.1016/j.jcomc.2023.100369.

[10] DeBorst R., Van den Bogert P.A.J., Zeilmaker, J. "Modelling and analysis of rubberlike materials." HERON, 33 (1), 1988 (1988)

[11] Pagani A. and Carrera E. Unified formulation of geometrically nonlinear refined beam theories. Mechanics of Advanced Materials and Structures, 25(1):15–31, sep 2016, DOI: 10.1080/15376494.2016.1232458.

[12] Holzapfel G.A. Nonlinear Solid Mechanics. John Wiley & Sons, Chichester, West Sussex, UK, 2000.

[13] Chiaia P., Pagani A., Cinefra M., and Carrera E. Analysis of transversely isotropic compressible and nearly-incompressible soft material structures by high order unified finite elements. Mechanics of Advanced Materials and Structures, pages 1–17, November 2023, DOI: 10.1080/15376494.2023.2273962.

[14] Carrera E., Cinefra M., Zappino E., and Petrolo M. Finite Element Analysis of Structures Through Unified Formulation. Wiley, Wiley, Chichester, West Sussex, UK, jul 2014.

[15] Carrera E. and Demasi L. Classical and advanced multilayered plate elements based upon PVD and RMVT. part 1: Derivation of finite element matrices. International Journal for Numerical Methods in Engineering, 55(2):191–231, June 2002, DOI: 10.1002/nme.492.

[16] Carrera E., Miglioretti F., and Petrolo M. Accuracy of refined finite elements for laminated plate analysis. Composite Structures, 93(5):1311–1327, April 2011, DOI: 10.1016/j.compstruct.2010.11.007.

[17] Wu B., Pagani A., Filippi M., Chen W.Q., and Carrera E. Accurate stress fields of post-buckled laminated composite beams accounting for various kinematics. International Journal of Non-Linear Mechanics, 111:60– 71, May 2019, DOI: 10.1016/j.ijnonlinmec.2019.02.002.

[18] Wu B., Pagani A., Filippi M., Chen W.Q., and Carrera E. Large-deflection and post-buckling analyses of isotropic rectangular plates by carrera unified formulation. International Journal of Non-Linear Mechanics, 116:18–31, November 2019, doi: 10.1016/j.ijnonlinmec.2019.05.004.

[19] Carrera E. Theories and finite elements for multilayered plates and shells: A unified compact formulation with numerical assessment and benchmarking. Archives of Computational Methods in Engineering, 10(3):215–296, September 2003, DOI: 10.1007/BF02736224.

[20] Carrera E, Pagani A., Petrolo M., and Zappino E. Recent developments on refined theories for beams with applications. Mechanical Engineering Reviews, 2(2):14–00298–14–00298, 2015, DOI: 10.1299/mer.14-00298.

[21] Pagani A. and Carrera E. Unified one-dimensional finite element for the analysis of hyperelastic soft materials and structures. Mechanics of Advanced Materials and Structures, 30(2):342–355, December 2021, DOI: 10.1080/15376494.2021.2013585.

[22] Reddy J. N. Introduction to Nonlinear Finite Element Analysis With Applica-

tions to Heat Transfer, Fluid Mechanics, and Solid Mechanics. Oxford University Press, New York, 2014.

[23] Pagani A., Chiaia P., and Carrera E. Vibration of solid and thin-walled slender structures made of soft materials by high-order beam finite elements. International Journal of Non-Linear Mechanics, 160:104634, April 2024, DOI: 10.1016/j.ijnonlinmec.2023.104634.

[24] Beheshti A and Ansari R. Finite element analysis of compressible transversely isotropic hyperelastic shells. Acta Mechanica, mar 2023, DOI: 10.1007/s00707-023-03536-z.